Desalination and Water Treatment
www.deswater.com

doi: 10.5004/dwt.2017.20586

75 (2017) 18–25
May

Comparative assessment of polyvinylpyrrolidone type of membranes based on porosity analysis

Małgorzata Przytulska[a,*], Aleksandra Kruk[b], Juliusz L. Kulikowski[a], Cezary Wojciechowski[a], Agnieszka Gadomska-Gajadhur[b], Andrzej Chwojnowski[a]

[a]*Laboratory of Fundamentals of Computer-Aided Image Diagnostics and Department of Biomedical System and Technologies, Nałęcz Institute of Biocybernetic and Biomedical Engineering Institute of Biocybernetics and Biomedical Engineering, Trojdena 4 str. O2-109 Warsaw, Poland, Tel. +48 22 5925950; Fax: +48 22 6597030; emails: mprzytulska@ibib.waw.pl (M. Przytulska), jkulikowski@ibib.waw.pl (J.L. Kulikowski), cwojciechowski@ibib.waw.pl (C. Wojciechowski), achwojnowski@ibib.waw.pl (A. Chwojnowski)*
[b]*Laboratory of Technological Processes, Faculty of Chemistry, Warsaw University of Technology, Warsaw, Poland, emails: akruk@ch.pw.edu.pl (A. Kruk), agadomska@ch.pw.edu.pl (A. Gadomska-Gajadhur)*

Received 26 October 2016; Accepted 13 February 2017

ABSTRACT

A method for computer-aided assessment of the quality of membranes in their production process is presented in this paper. The method is based on computer analysis of the scanning electron microscope (SEM) images of membrane's sections. A novelty of the method consists in fully automatic identification, contouring, size measuring and classification of the pores in SEM images of the specimens of the membranes. Two defined in the paper parameters, general porosity factor and inner penetration factor, in long series of images corresponding to the membranes produced by a given technological method for membrane's quality evaluation or for comparison of membranes produced by different methods are proposed. The proposed method was used to the assessment of the porosity of poly-L-lactide membranes obtained by the inversion phase method. The analyzed membranes were intended for use as scaffolds for culturing specific biological tissues (chondrocytes for cartilage lesion regeneration). Experimental results of the assessment of two types of membranes produced by alternative methods are presented. Plans for future work aimed at the improvement and extension of the method to a larger set of morphological parameters characterizing the porosity of membranes are presented.

Keywords: Poly-L-lactide membranes; Morphological parameters; Porosity evaluation; Computer-aided image processing; 3-D scaffold

1. Introduction

Porous materials and scaffolds of various shapes and forms are important for many technological (bioreactors [1], water filters [2,3], etc.), medical (plasma fractioning [4], blood detoxification by dialysis [5]) or biotechnological [6–9] applications. In tissue engineering porous materials can provide a temporary microenvironment to promote cell adhesion, proliferation and differentiation to guide the formation of new tissues and organs [10–13]. Biodegradable and stable polymers, ceramics and their composites have been formed into porous structures for use in tissue engineering [14–17]. Controlling the pore structure, including pore size and interconnectivity, is one of the more important problems and key to creating porous biomaterials that are ideal as scaffolds [18–22]. Cell functions and new tissue regeneration rely heavily on the size of the pores. Many studies have demonstrated the effects of the pore size of a porous scaffold on tissue regeneration [24–30]. Some results indicate that phenotype and biosynthetic activity of chondrocytes is improved in collagen matrices containing smaller pores [26,29]. Generally

* Corresponding author.

the pore size should be in a range that facilitates cell penetration and migration during cell seeding and provides a three-dimensional (3-D) microenvironment inducing cell assembly and differentiation. On the other hand, pores in scaffolds should ensure the ease of nutrient diffusion and removal. In general, large pores are more easily accessible to chondrocytes than small pores [24,26–28].

In preparing porous scaffolds for chondrocyte cultivation it was found to be necessary to have an objective method for assessing the porosity of the scaffold. It is widely accepted that the pore size is an important factor in determining the properties of porous materials. However, the pores are of various irregular shape, size and spatial distribution. Information about their properties is available mainly from two-dimensional sections of the specimens of materials under investigation. The problem addressed was the development of a computer-based image analysis method of quality assessment for porous materials, which takes into account the specific, multi-level and irregular nature of each material's porosity. The aim is to present a solution to this problem based on the morphological segmentation of various classes of pores combined with statistical analysis of their parameters. The resultant method is a combination of several existing image-processing techniques. However, these have been brought together to produce a compact and specialized image analysis technique based on the results of a series of experiments, which were aimed at the selection of subprocedures and their parameters to give the most suitable solution for the given problem. It was shown in reference [31] that computer-based microscopic image analysis can be an effective tool for the quality assessment of porous materials.

In this paper the method has been extended to a wider class of porous materials. Moreover, the method of pores selection has been modified: (a) the selection of pores into size-classes is automatically performed without using the transitional, coloured form of images (used in reference [31]), (b) the pre-processing of images has been improved by including morphological operations and (c) a watershed splitting approach (consisting of viewing the image as a "mountain profile" filled from the bottom by water whose rising level floods the hollows and marks out their borders) has been modified by using adaptive threshold level and has been used to the selection of pores. The so-modified method makes a partition of pores into size-classes more reliable.

The paper is organized as follows. The materials studied are described in section 2. Section 3 describes the methods used and consists of three subsections. The first subsection describes the technique for producing the membranes. The second subsection presents the methods used to prepare the microscopic specimens and to acquire the images. The third subsection describes computer-based method for assessing the porosity of the membranes. Section 4 presents the results of experiments illustrating the effectiveness of the proposed membrane porosity assessment method. Concluding comments and proposals for future work are given in section 5.

2. Materials

The components, (a) poly-L-lactide (PLLA), M_n 86,000 g/mol, NatureWorks NW 2003D, (b) polyvinylpyrrolidone (PVP), M_n 10,000 g/mol and (c) Pluronic® F127 purchased from Sigma Aldrich (Poland (branch) Ltd. 61-626 Poznań, Szelągowska 30 str.) were used to prepare membranes. Chloroform produced by POCh (Poland 44-101 Gliwice, Sowińskiego 11 str.) SA was used as the solvent. Ultrapure water with 18.2 MΩcm conductivity was obtained using a Milli-Q device. Polymer nano-non-wovens were obtained using an electrospinning technique with pork skin gelatin type A from Sigma Aldrich.

The image-processing methods were tested on a series of scanning electron microscope (SEM) images of the sections of the examined materials. The samples were coated with a 7–10 nm of gold using a K550X Sputter Coater apparatus. Images were taken at 300× and at 1,000× magnification using a Hitachi TM1000 SEM with a 15-kV acceleration voltage.

3. Methods

3.1. Membranes production

The membranes were obtained using the inversion phase method. PLLA was dissolved in chloroform with constant stirring for 24 h to give a 6 wt% solution. The pore precursors were then added. These were either PVP (with weight ratio PLLA:PVP 1:1), in membrane type I or PVP, and Pluronic® (with weight ratio PLLA:PVP:Pluronic® 100:100:25), in membrane type II.

The membrane-forming solution was then poured onto a glass plate. Gelatin nano-non-woven was placed onto the solution layer after pouring, and the air was removed by applying pressure. Another layer of solution was then poured, and nano-non-woven was placed on top once again. The air was again removed. The membrane was then gelled in methanol at –18°C. After the gelling bath a washing (aqueous) bath was used to eliminate polymeric nano-non-wovens. Following polymer coagulation and the removal of pore precursors, the membrane was dried.

3.2. Preparation of the specimens and microscopic image acquisition

Samples of the membranes were immersed in ethanol, frozen in liquid nitrogen and then fractured in liquid nitrogen. After drying they were coated with a 7–10 nm thick gold layer using a K550X Sputter Coater. The gold-coated samples were viewed and recorded using an scanning electron microscope (SEM). Fig. 1 shows an SEM image of a sample of porous membrane: (a) magnified 300×, (b) part of it further electronically magnified by a factor of two and (c) the surface plot (or 3-D plot created as a 3-D representation of the intensity of an image).

Two features of the image are immediately notable. Firstly, the pores consist of small, almost circular, and large, very irregular forms. Secondly, despite the fact that a two-dimensional section of the sample is visualized, the gradation of darkness inside the large pores (more visible in the magnified fragment) provides some information about their 3-D morphological structure.

As can be seen in Figs. 2(a) and (b), the morphological structure in the two types of membranes specified in section 3.1 is different.

Extraction from the image of information on their 3-D morphological structure is a challenge for computer-based

image analysis methods. In particular the ratio of small to large pores is a significant factor in determining the membrane's physical and biomedical properties. The two alternative types of membranes were then assessed and compared, as it will be described in section 4 of the paper.

3.3. Computer analysis of images

The image analysis procedure consists of two stages: image pre-processing and image processing. These are shown in Fig. 3. Both stages are composed of suitable subprocedures taken from the Image Pro Plus library and adjusted for the given problem.

The aim of the image pre-processing is to present the image in a standard form thus reducing the number of systematic errors at the main image analysis stage.

Pre-processing consists of a series of standard operations including image calibration (presentation on a standard scale of pixels/mm); the selection of the areas of interest (AOI); noise reduction by median 3 × 3 filtering; contrast enhancement by equalization of the luminance histogram; contour enhancement by HIGAUSS 7 × 7 filtering; and pore separation by morphological closing of contours using the MORPHO_3 ×3 CROSS structural element [32–35].

The result of image pre-processing is shown in Fig. 4. The structure of the pores, i.e., their differentiation into small and large pores and the irregularity of shapes of the large pores, becomes more clear. Moreover, the spatial form of large pores has been visualized.

The main image-processing stage consists of the extraction from the images corrected in the pre-processing stage of information describing the morphological structure of the examined membrane. Pore segmentation, based on adaptive thresholding, takes into account the fact that pores in the image are darker than in the background. To do this the image was partitioned into smaller areas, and any pixel whose luminance did not exceed the mean luminance level in a given area was classified as belonging to pores. Watershed splitting consists of viewing the image as a "mountain profile" filled from the bottom by water whose rising level floods the hollows and marks out their borders. The limited watershed method used in our work eroded objects only up to a certain luminance level.

Standard image-processing procedures allow various criteria for the selection and counting of objects. In our case, at the first stage of investigation, it was decided:

- to use the objects' area, due to its numerical simplicity, for object selection;
- to neglect the objects contiguous to the image borders as undefined in form and size;

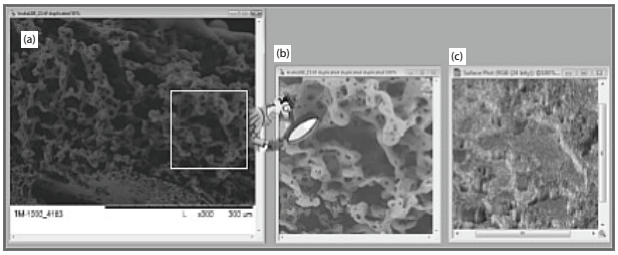

Fig. 1. Example of an SEM image of a sample of porous membrane: (a) magnified 300×, (b) part of it further electronically magnified by a factor of two and (c) the surface plot (created as a three-dimensional representation of the intensity of an image).

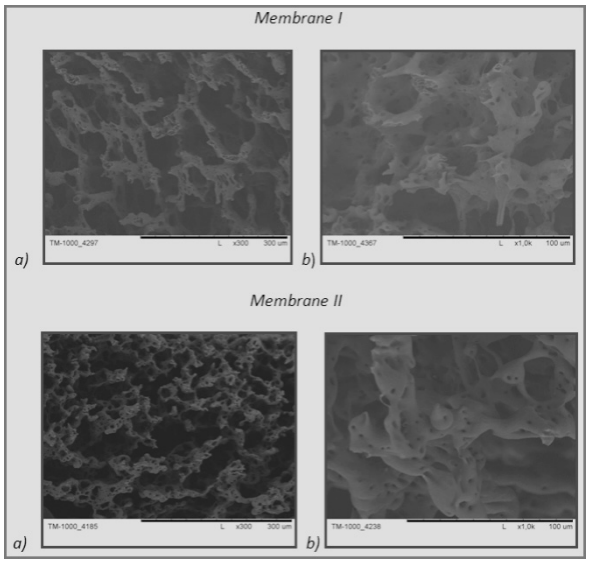

Fig. 2. SEM images of type I and type II of membranes: (a) 300× magnified and (b) 1,000× magnified.

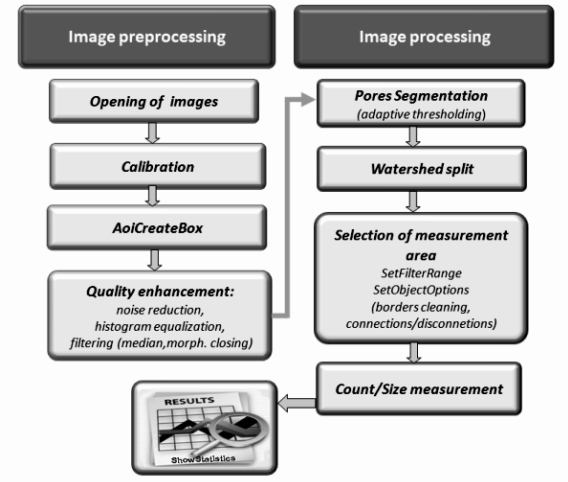

Fig. 3. General image analysis procedure.

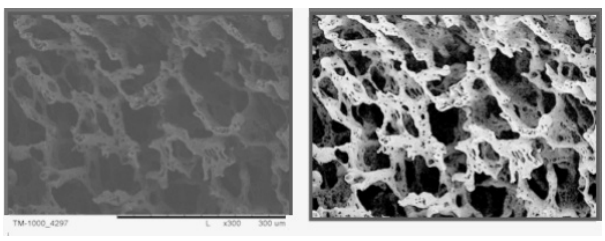

Fig. 4. Example of the effects of image pre-processing: (a) source image and (b) enhanced image.

- to use the eight-connectivity concept as the objects' connection/disconnection criterion; and
- to divide the pores into five area classes.

The size of irregular pores can be defined in various ways such as the length of the major axis, the minimum covering *XY* box area or the maximum covered inner circle area or diameter. In our case the exact area of the pores is calculated as proportional to the number of pixels filling the contour of the area. This was used to discriminate the following area classes of pores: 1–3 μm², 3–8 μm², 8–20 μm², 20–80 μm² and >80 μm².

Typical image-processing procedures also allow choices between including and neglecting objects with holes, objects adjacent to image borders, etc. This is illustrated in Fig. 5.

Finally, any selected class of objects, if necessary, can be distinguished, as shown in Fig. 6, where the pores 1–3 μm² size have been selected.

For the selected class of objects typical statistical parameters, the mean and standard deviation of their area can be calculated. However, note that, at this stage of investigation, no shape characteristics of pores have been considered.

4. Experimental results and discussion

The experiments described below were aimed at testing the usefulness of basic morphological parameters in characterizing various classes of pores and in discriminating between membranes produced by the two methods described in section 3.1. According to the fact that in our case different roles are played in the membranes by small (0–20 μm²) and large (>20 μm²) areas, the quality of membranes should be evaluated by analysis of different size-classes of pores. In general, we are interested in obtaining membranes characterized by low standard deviation of the size in each size-class of pores. On the other hand, the quality of a technological process is characterized by the stability of statistical parameters of pores measured in long series of specimens and of images corresponding to a fixed type of membrane. This stability is characterized by standard deviations of the parameters measured in long series of the analyzed images. Also in this case the standard deviations are desired to be as small as possible.

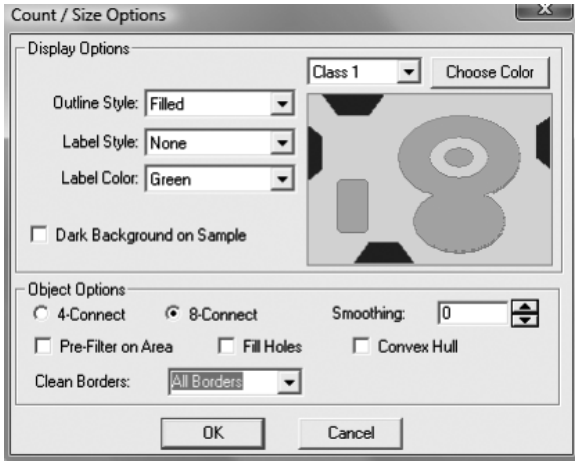

Fig. 5. Computer screen illustrating (in grey) the type of irregular objects taken into account in image analysis.

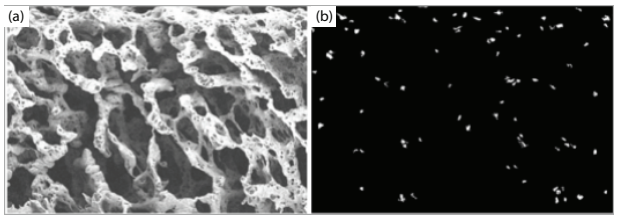

Fig. 6. Results of selected 0–3 μm² size objects: (a) original image and (b) selected objects.

4.1. Experiment 1

The aim of this experiment was evaluation of the porosity of membranes as one of their quality parameters, measured over long series of images acquired from each type of membrane. It should be noted that the magnification used for the SEM images of 1,000× was chosen as a compromise between good visibility of the pores and the number of large pores available for statistical analysis. Both types of membranes were used. For each 20 images taken from 3 membrane specimens were analyzed. The morphological parameters measured were the total area of pores and total image area. The results are averaged over the series of images representing a given type of membrane.

The general porosity factor (GPF) of a membrane can be defined as:

$$\mathrm{GPF} = \frac{\text{total area of pores}}{\text{total image area}} \cdot 100\% \quad (1)$$

In Fig. 7 the measured and calculated GPF values of two alternative membranes are presented.

The areas were calculated as proportional to the number of pixels filling the contour of the area.

The GPF values for membrane I are between 33% and 44% while for membrane II they are between 37% and 42%. This is visible in Fig. 8 where the GPFs averaged over all of the images for each membrane type are shown.

Note that the standard deviation of the GPF in both cases is <4% of the mean value. At this state of investigations any threshold levels cannot be established but in an intuitive way, they need to be verified in the future on the basis of biomedical experiments. Here, it has been preliminarily assumed that if the standard deviation of the GPF is >10% then this suggests that the technological process is not sufficiently

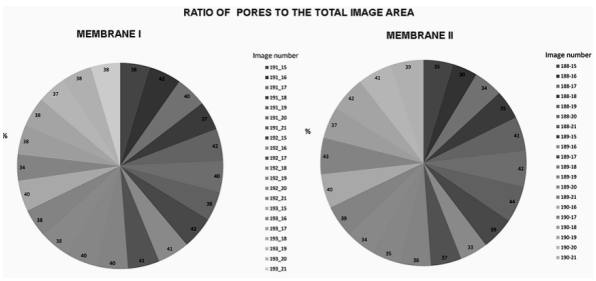

Fig. 7. General porosity factors (GPF) of series of images representing two types of membranes.

stable. Under this assumption, the calculated values of the GPF show that both alternative technologies of membrane production are sufficiently stable. Moreover, the porosity of membrane I seems to be less homogenous than that of membrane II, because of its two times greater standard deviation. This point will be deeply investigated in the Experiment 3.

4.2. Experiment 2

In this experiment the possibility of automatic image segmentation and of classification of pores according to their area was tested on typical SEM images. The size-classes of pores have been fixed by standard image analysis program. An example is shown in Fig. 9.

Selected measured parameters characterizing the classes of pores are given in Table 1. The number of classes and the results of classification are here different from those presented in reference [31], where the size-classes were chosen in arbitrary way. The process of segmentation of pores used here is presented in Fig. 3.

The functional role of small and large pores in a membrane is different. Small pores convey germinal cells and alimentary substances to the large pores where the colonies of chondrocytes should grow. The distribution of sizes of pores and their connectivity is described by the inner penetration ability. To quantify the inner penetration ability, inner penetration factors (IPF) can be defined for a membrane:

$$\mathrm{IPF1} = \frac{\text{number of small } (\leq 3\ \mu m^2) \text{ pores}}{\text{number of middle size } (20 \ldots 80\ \mu m^2) \text{ pores}} \quad (2a)$$

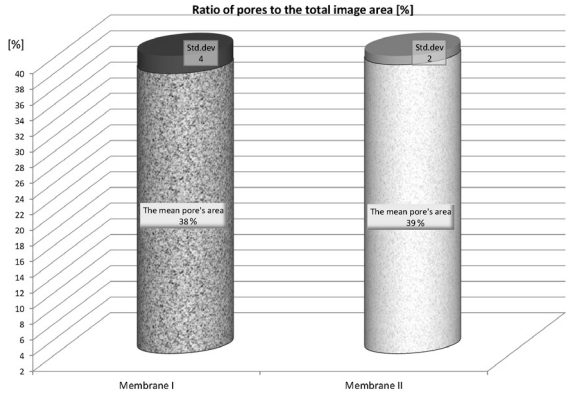

Fig. 8. The GPF values in two alternative membranes: bottom parts – mean values and top parts – standard deviations.

or

$$\mathrm{IPF2} = \frac{\text{number of small } (\leq 3\ \mu m^2) \text{ pores}}{\text{number of large } (> 80\ \mu m^2) \text{ pores}} \quad (2b)$$

Table 2 shows the relationship between the values of IPF2 and the four corresponding classes of penetration ability. In this case these have been intuitively chosen. In future they should be established on the basis of observation of real colonies of chondrocytes growing on the PLLA membrane scaffolds. In this experiment the calculated value of IPF2 is 64.8, which qualifies the given membrane's inner penetration ability as good.

This experiment has demonstrated the possibility of simple automatic measurement of some of the parameters, which characterize a membrane's porosity. However, in order to use the image-processing methods to evaluate the quality of membranes, a much larger number of images should be assessed.

4.3. Experiment 3

In this experiment the computer-aided image-processing method was used to compare the basic morphological parameters of the two types of membranes. For this purpose, two series of SEM images of two types of membranes have been analyzed and compared.

Analysis of the basic morphological parameters, such as those shown in Table 1, of a selected class of pores, gives an assessment of the quality of membranes specimen. The results for the 0–3 μm² class of pores are shown in Fig. 10.

The minimum and maximum areas of pores are limited by the definition of the given size-class of pores. If the

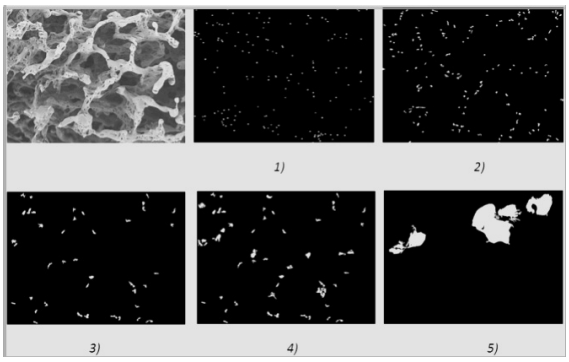

Fig. 9. Result of automatic image segmentation discriminating between the 5 classes of pores.

Table 1
Selected parameters of automatically discriminated 5 classes of pores

Class	Range of area, μm²	Number of objects	Percentage of objects	Total area, μm²	Percentage of area	Mean area	Standard deviation of area	Min. area, μm²	Max. area, μm²
1	0–3	165	44.35	358.24	6.64	2.17	0.45	0.76	2.88
2	3–8	150	40.32	665.47	12.33	4.44	1.37	3.04	7.89
3	8–20	40	10.75	503.20	9.33	12.58	3.77	8.05	19.89
4	20–80	12	3.23	393.46	7.29	32.79	12.92	20.34	60.41
5	>80	5	1.34	3,474.76	64.41	694.95	575.82	183.98	1801.51

number of pores in an observation area is very large then the probability distribution of their size streams to be uniform in the given interval. Its standard deviation then becomes close to its theoretical maximal value given by the formula:

$$\sigma = \frac{d^{3/2}}{2\sqrt{3}} \cong 0.287 d^{3/2} \quad (3)$$

where d denotes the lengths of the interval. In the given case the measured, real lowest intervals are 0.593–2.966 μm² in membrane I and 0.457–2.892 μm² in membrane II. The corresponding lengths of intervals are then 2.373 and 2.435 μm². The calculated standard deviations for the corresponding uniform distributions should thus be, respectively, 1.049 and 1.091 μm². In fact, their averaged over the series of images values are 0.686 in membrane I and 0.679 in membrane II. This means that the probability distributions of areas measured in the real lowest intervals are not exactly uniform. Moreover, the measured mean areas additionally averaged over the series of images equal 1.475 in membrane I and 1.468 in membrane II. The difference, in the third decimal position, seems to be not significant. However, the dispersion D of measured standard deviations is defined as:

$$D = Av\left(\max.\text{st.dev} - \min.\text{st.dev}\right) \quad (4)$$

where Av denotes arithmetical averaging of the differences between standard deviations of the areas of pores over a series of images corresponding to a given type of membrane, leads to the result: $D_I = 0.127$ in membrane I and $D_{II} = 0.048$ in membrane II. This shows that the stability of the areas of the smallest pores in membrane II is 2.6 times greater than in membrane I.

Similar statistical analysis of the areas of pores in other classes of pores has been done. In general, it is desirable that the dispersion D in all classes of pores does not exceed a certain limit of the mean area in the given class of pores. The graphs in Figs. 11 and 12, where the mean values and standard deviations of the areas of pores are, respectively, plotted, show that this requirement can be particularly difficult to be satisfied in the class of the largest (>80 μm²) pores. In the (20–80 μm²) class of pores the arithmetically averaged over the series of images mean areas are 36.94 μm² in membrane I and 37.15 μm² in membrane II, while the corresponding geometrically averaged standard deviations are, respectively, 15.54 and 15.09 μm², respectively. This means that the standard deviation to mean value ratios are 0.421 in membrane I and 0.406 in membrane II. In both cases, as <0.5, they are admissible for a preliminary assessment of the quality of membranes. However, it follows from a comparison of the data that the difference of the quality of the membranes is statistically not

Table 2
IPF2 values used to membranes' inner penetration ability evaluation

IPF2	Penetration ability
<10	Bad
10–49	Unsatisfactory
50–149	Good
≥150	Very good

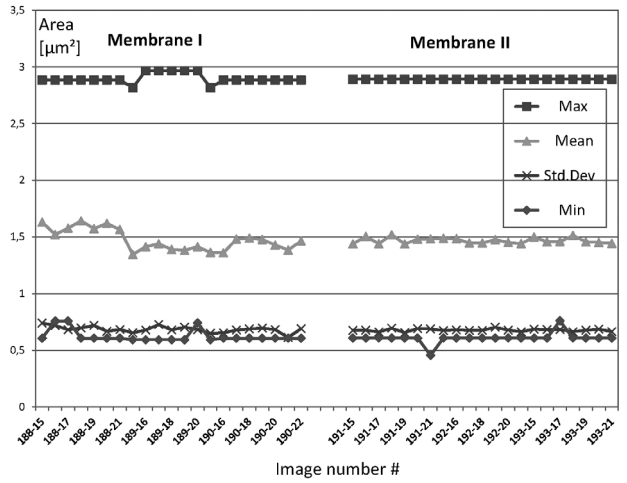

Fig. 10. Measured basic parameters of the 0–3 μm² class of pores.

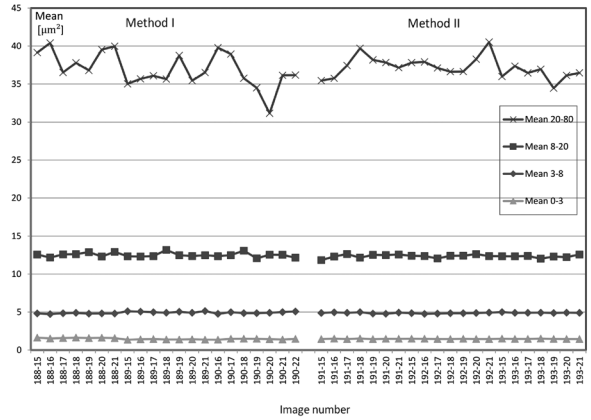

Fig. 11. Mean pore areas in the series of images for two membrane types and four size-classes.

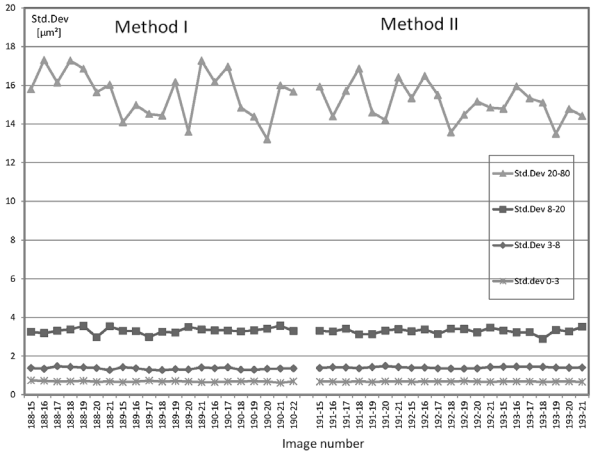

Fig. 12. Standard deviations of pore areas in the series of images for two membrane types and four size-classes.

significant. It also follows from the obtained data that using very highly (>1,000×) magnified SEM images to analysis of the largest pores cannot be recommended because in such case much higher standard deviations of the size of pores can be expected and longer series of images should be analyzed in order to evaluate the parameters of pores on a satisfactory accuracy level.

In order to evaluate the stability of the membranes' parameters in long series of images, the standard deviations of the mean values of pore size for the series have been calculated. The values obtained are 2.25 μm² in membrane I and 1.37 μm² in membrane II, as shown in Fig. 13, where the values are presented with the corresponding averaged mean values. It is visible that the stability of membrane II is 1.64 times higher (the standard deviation is 0.61 times lower) than this of membrane I.

At last, the inner penetration factors IPF1 and IPF2 of the two membrane types were measured and calculated. The results presenting the values of the factors in two series of images (21 images long) are shown in Fig. 14.

The averaged over the series of images values of IFP1 are: 0.040 in membrane I and 0.0396 in membrane II, while the corresponding averaged standard deviations are 0.002, 0.0028, 0.0014 and 0.00156. Similarly, the averaged over the series of images values of IFP2 are: 0.0396 in membrane I and 0.0016, 0.0018 in membrane II, while the corresponding averaged standard deviations are 0.0018, 0.0014 and 0.00065. This means that there is no substantial difference between the averaged IPFs in the two membranes; however, the averaged standard deviations of the IFPs are evidently lower in membrane II than in membrane I.

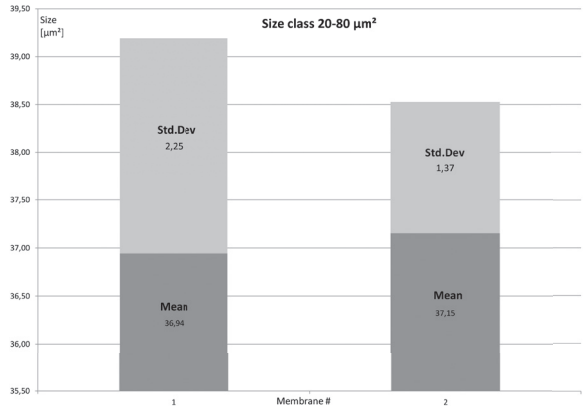

Fig. 13. Comparison of the mean pore areas in the 20–80 μm² class of pores, averaged in the series of images (lower segments) and of their variances calculated in the series (upper segments).

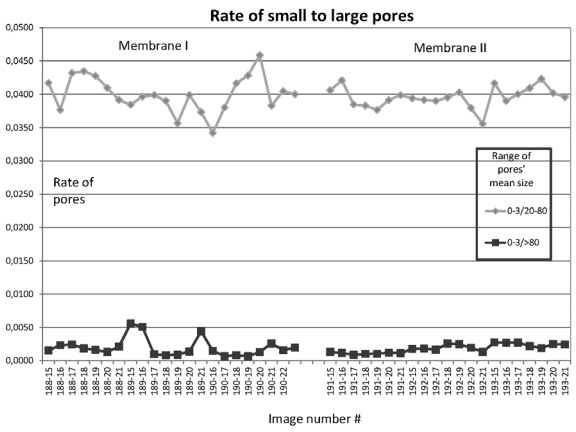

Fig. 14. The measured and calculated IPF1 (upper curves) and IPF2 (lower curves) for the two membranes.

5. Conclusions

PVP membranes can be used for the construction of scaffolds for cartilage cell cultures. For this application their porosity is very important and should be carefully controlled during the production process. To this end SEM imaging technology combined with computer-aided methods of image analysis can be used to gain insight into the morphological structure of the membranes. The diversity of size and the irregularity of form of the pores necessitate the use of specific morphological and statistical methods in order to describe them. Computer-aided image-processing methods have the further advantage that they are suitable for the automation of the process of assessing the porous membranes. In particular they make possible the segmentation and classification of the pores according to their area, and the counting of the pores of each size observable in the image frame.

However, small and large pores play different roles in cartilage cell cultures, and the corresponding classes of pores need to be independently analyzed. The mean value and standard deviation of the area of segmented pores can be used as basic parameters characterizing the quality of membranes. In particular, they make possible to compare the quality of membranes produced by two (or more) alternative methods and to control the stability of basic morphological parameters of membranes produced by a given technological process. However, the technique proposed in this work, which is based on a rough classification of the parameters to determine the quality of membranes, needs to be refined by taking into account the results of forthcoming experiments where real colonies of chondrocytes on PLLA membrane scaffolds are cultured.

The brittleness of the material makes getting several adjacent sections of a membrane for numerical analysis impossible. Therefore, genuine 3-dimensional morphological membrane analysis will require more sophisticated theoretical models and based on them methods, like those described in [23], for reconstructing the absent third dimension of large pores, on the basis of their luminance profile. A local image darkness level provides information about relative depth of a pore under consideration. The membrane's properties following from the 3-D membrane's morphological structure will be the topic of a forthcoming paper under preparation.

Acknowledgements

The work described in this paper was carried out as part of a project ST/1614 financed by the Nalecz Institute of Biocybernetics and Biomedical Engineering, Polish Academy of Sciences, Warsaw. The authors would like to acknowledge the assistance of Diana Wierzbicka M.Sc. in preparation of graphical objects. We also appreciate the helpful comments on the drafting of the paper provided by the proof reading service.

Symbols

GPF	—	General porosity factor
IPF1 and IPF2	—	Inner penetration factors
σ	—	Standard deviation
d	—	Length of interval
D	—	Dispersion

References

[1] N. Thongmak, P. Sridang, U. Puetpaiboon, M. Héran, G. Lesage, A. Grasmick, Performances of a submerged anaerobic membrane bioreactor (AnMBR) for latex serum treatment, Desal. Wat. Treat., 57 (2016) 20694–20706.

[2] M.A.H. Johira, W.G. Shimb, M. Pradhana, S. Vigneswarana, J. Kandasamya, Benefit of adding adsorbent in submerged membrane microfiltration treatment of wastewater, Desal. Wat. Treat., 57 (2016) 20683–20693.

[3] J. Tian, H. Yu, Y. Shen, W. Shi, D. Liu, S. Gao, F. Cui, Identification of irreversible UF membrane foulants by fluorescence excitation–emission matrix coupled with parallel factor analysis, Desal. Wat. Treat., 57 (2016) 21794–21805.

[4] A. Sueoka, Present status of apheresis technologies: Part 2. Membrane plasma fractionator, Ther. Apher. Dial., 1 (1997) 135–146.

[5] F. Locatelli, F. Mastrangelo, B. Redaelli, C. Ronco, D. Marcelli, G. La Greca, G. Orlandini, Effects of different membranes and dialysis technologies on patient treatment tolerance and nutritional parameters. The Italian Cooperative Dialysis Study Group, Kidney Int., 50 (1996) 1293–1302.

[6] C.H. Wu, F.K. Lee, S. Suresh Kumar, Q.D. Ling, Y. Chang, Y. Chang, H.-C. Wang, H. Chen, D.-C. Chen, S.-T. Hsu, A. Higuchi, The isolation and differentiation of human adipose-derived stem cells using membrane filtration, Biomaterials, 33 (2012) 8228–8239.

[7] A. Higuchi, Q.D. Ling, S.T. Hsu, A. Umezawa, Biomimetic cell culture proteins as extracellular matrices for stem cell differentiation, Chem. Rev., 112 (2012) 4507–4540.

[8] S.J. Hollister, Porous scaffold design for tissue engineering, Nat. Mater., 4 (2005) 518–524.

[9] P.Y. Wang, L.R. Clements, H. Thissen, A. Jane, W.B. Tsai, N.H. Voelcker, Screening mesenchymal stem cell attachment and differentiation on porous silicon gradients, Adv. Funct. Mater., 22 (2012) 3414–3423.

[10] H. Lu, N. Kawazoe, T. Kitajima, Y. Myoken, M. Tomita, A. Umezawa, G. Chen, Y. Ito, Spatial immobilization of bone morphogenetic protein-4 in a collagen-PLGA hybrid scaffold for enhanced osteoinductivity, Biomaterials, 33 (2012) 6140–6146.

[11] R. Balen, W. Vidotto de Costa, J. De Lara Andrade, J.F. Piai, E.C. Muniz, M.V. Companhoni, T.U. Nakamura, S.M. Lima, L.H. Andrade, P.R. Stival Bittencourt, A. Hechenleitner, E.A.G. Pineda, D.M. Fernandes, Structural, thermal, optical properties and cytotoxicity of PMMA/ZnO fibers and films: potential application in tissue engineering, J. Appl. Polym. Sci., 385 (2016) 257–267.

[12] G.C. Engelmayr, M. Cheng, C.J. Bettinger, J.T. Borenstein, R Langer, L.E. Freed, Accordion-like honeycombs for tissue engineering of cardiac anisotropy, Nat. Mater., 7 (2008) 1003–1010.

[13] A. Kinasiewicz, K. Dudziński, A. Chwojnowski, A. Weryński, J. Kawiak, Three-dimensional culture of hepatocytes on spongy polyethersulfone membrane developed for cell transplantation, Transplant. Proc., 39 (2007) 2914–2916.

[14] E.C. Ko, Y. Fujihara, T. Ogasawara, Y. Asawa, S. Nishizawa, S. Nagata, et al., BMP-2 embedded atelocollagen scaffold for tissue-engineered cartilage cultured in a medium containing insulin and triiodothyronine—a new protocol for three-dimensional in vitro culture of human chondrocytes, Tissue Eng. Part C, 18 (2012) 374–386.

[15] Y. Tanaka, H. Yamaoka, S. Nishizawa, S. Nagata, T. Ogasawara, Y. Asawa, Y. Fujihara, T. Takato, K. Hoshi, The optimization of porous polymeric scaffolds for chondrocyte/atelocollagen based tissue-engineered cartilage, Biomaterials, 31 (2010) 4506–4516.

[16] M. Płończak, J. Czubak, G. Hoser, A. Chwojnowski, J. Kawiak, K. Dudziński, K. Czumińska, Repair of articular cartilage full thickness defects with cultured chondrocytes placed on polysulphonic membrane – experimental studies in Rabbits, Biocyb. Biomed. Eng., 28 (2008) 87–93.

[17] C.C. Chen, W.C. Wang, S.J. Ding, In vitro physiochemical properties of a biomimetic gelatin/chitosan oligosaccharide/calcium silicate cement, J. Biomed. Mater. Res. Part B, 95 (2010) 456–465.

[18] K.A. Faraj, T.H.V. Kuppevelt, W.F. Daamen, Construction of collagen scaffolds that mimic the three-dimensional architecture of specific tissues, Tissue Eng., 13.(2007) 2387–2394.

[19] M.M.C.G. Silva, L.A. Cyster, J.J.A. Barry, X.B. Yang, R.O.C. Oreffo, D.M. Grant, C.A. Scotchford, S.M. Howdle, K.M. Shakesheff, F.R.A.J. Rose, The effect of anisotropic architecture on cell and tissue infiltration into tissue engineering scaffolds, Biomaterials, 27 (2006) 5909–5917.

[20] K. Dudziński, A. Chwojnowski, M. Gutowska, M. Płończak, J. Czubak, E. Łukowska, C. Wojciechowski, Three dimensional polyethersulphone scaffold for chondrocytes cultivation – the future supportive material for articular cartilage regeneration, Biocybern. Biomed. Eng., 30 (2010) 65–76.

[21] F.J. O'Brien, B.A. Harley, I.V. Yannas, L.J. Gibson, The effect of pore size on cell adhesion in collagen-GAG scaffolds, Biomaterials, 26 (2005) 433–441.

[22] T.B. Woodfield, J. Malda, J. De Wijn, F. Péters, J. Riesle, C.A. van Blitterswijk, Design of porous scaffolds for cartilage tissue engineering using a three-dimensional fiber-deposition technique, Biomaterials, 25 (2004) 4149–4161.

[23] H. Li, J. Wang, Q. Shi, M. Zhang, C. Hou, G. Shi, H. Wang, Q. Zhang, Y. Li, Q. Chi, Constructing three-dimensional quasi-vertical nanosheet architectures from self-assemble two-dimensional $WO_3 \cdot 2H_2O$ for efficient electrochromic devices, App. Surf. Sci., 385 (2016) 257–267.

[24] C.M. Murphy, M.G. Haugh, F.J. O'Brien, The effect of mean pore size on cell attachment, proliferation and migration in collagen-glycosaminoglycan scaffolds for bone tissue engineering, Biomaterials, 31 (2010) 461–466.

[25] S. Nuernberger, N. Cyran, C. Albrecht, H. Redl, V. Vécsei, S. Marlovits, The influence of scaffold architecture on chondrocyte distribution and behavior in matrix associated chondrocyte transplantation grafts, Biomaterials, 32 (2011) 1032–1040.

[26] H. Stenhamre, U. Nannmark, A. Lindahl, P. Gatenholm, M. Brittberg, Influence of pore size on the redifferentiation potential of human articular chondrocytes in poly(urethane urea) scaffolds, J. Tissue Eng. Regener. Med., 5 (2011) 578–588.

[27] S.M. Lien, L.Y. Ko, T.J. Huang, Effect of pore size on ECM secretion and cell growth in gelatin scaffold for articular cartilage tissue engineering, Acta Biomater., 5 (2009) 670–679.

[28] S.H. Oh, I.K. Park, J.M. Kim, J.H. Lee, In vitro and in vivo characteristics of PCL scaffolds with pore size gradient fabricated by a centrifugation method, Biomaterials, 28 (2007) 1664–1671.

[29] M. Kawakami, N. Tomita, Y. Shimada, K. Yamamoto, Y. Tamada, N. Kachi, T. Suguro, Chondrocyte distribution and cartilage regeneration in silk fibroin sponge, Biomed. Mater. Eng., 21 (2011) 53–61.

[30] Q. Zhang, H. Lu, N. Kawazoe, G. Chen, Pore size effect of collagen scaffolds on cartilage regeneration, Acta Biomater., 10 (2014) 2005–2013.

[31] A. Chwojnowski, M. Przytulska, D. Wierzbicka, J.L. Kulikowski, C. Wojciechowski, Membrane's porosity evaluation by computer-aided analysis of SEM images, a preliminary study, Biocybern. Biomed. Eng., 32 (2012) 65–75.

[32] M. Sonka, V. Hlavac, R. Boyle, Image Processing Analysis and Machine Vision, Thomson, Toronto, 2008.

[33] J.C. Russ, The Image Processing Handbook, 6th ed., CRC Press, Boca Raton, 2011, pp. 433–506.

[34] I. Pitas, Digital Image Processing Algorithms and Applications, A Wiley-Interscience Publication, New York, 2013, pp. 323–334.

[35] W.K. Pratt, Digital Image Processing, John Wiley & Sons, New York, 2007.